

**GOES-East and
GOES-West AOD
retrieval**

H. Zhang et al.

This discussion paper is/has been under review for the journal Atmospheric Measurement Techniques (AMT). Please refer to the corresponding final paper in AMT if available.

Aerosol Optical Depth (AOD) retrieval using simultaneous GOES-East and GOES-West reflected radiances over the Western US

H. Zhang¹, R. M. Hoff¹, S. Kondragunta², I. Laszlo², and A. Lyapustin³

¹Joint Center for Earth Systems Technology (JCET), University of Maryland Baltimore County, Baltimore, MD, USA

²NOAA/NESDIS/STAR, College Park, MD, USA

³NASA/GSFC, Greenbelt, MD, USA

Received: 13 October 2012 – Accepted: 19 October 2012 – Published: 30 October 2012

Correspondence to: H. Zhang (hazhang@umbc.edu)

Published by Copernicus Publications on behalf of the European Geosciences Union.

Title Page

Abstract

Introduction

Conclusions

References

Tables

Figures

◀

▶

◀

▶

Back

Close

Full Screen / Esc

Printer-friendly Version

Interactive Discussion



Abstract

Aerosol Optical Depth (AOD) in the Western United States is observed independently by both the GOES-East and GOES-West imagers. The GASP (GOES Aerosol/Smoke Product) aerosol optical depth retrieval algorithm treats each satellite as a unique sensor and thus NOAA obtains two separate aerosol optical depth values at the same time for the same location. The TOA radiances and the associated derived optical depths can be quite different due to the different viewing geometries with large difference in solar-scattering angles. In order to fully exploit the simultaneous observations and generate consistent AOD retrievals from the two satellites, the authors develop a new aerosol optical depth retrieval algorithm that uses data from both satellites. The algorithm uses combined GOES-East and GOES-West visible channel TOA reflectance and daily average AOD from GOES Multi-Angle Implementation of Atmospheric Correction (GOES-MAIAC) on clear days (AOD less than 0.3), when diurnal variation of AOD is low, to retrieve surface BRDF. The known BRDF shape is applied on subsequent days to retrieve BRDF and AOD. The algorithm is validated at three AERONET sites over the Western US. The AOD retrieval accuracy from the hybrid technique using the two satellites is similar to that from one satellite over UCSB and Railroad Valley. Improvement of the accuracy is observed at Boulder. The correlation coefficients between the GOES AOD and AERONET AOD are in the range of 0.67 to 0.81 over the three sites. The hybrid algorithm has more data coverage compared to the single satellite retrievals over surfaces with high reflectance. The number of coincidences with AERONET observations increases from the use of two-single satellite algorithms by 5–80 % for the three sites. With the application of the new algorithm, consistent AOD retrievals and better retrieval coverages can be obtained using the data from the two GOES satellite imagers.

GOES-East and GOES-West AOD retrieval

H. Zhang et al.

Title Page

Abstract

Introduction

Conclusions

References

Tables

Figures

◀

▶

◀

▶

Back

Close

Full Screen / Esc

Printer-friendly Version

Interactive Discussion



1 Introduction

Atmospheric aerosol is an important component of climate change and public health research. Aerosols radiatively force climate through the direct and several indirect effects (Charlson et al., 1992; Kiehl and Briegleb, 1993; Ramanathan et al., 2001; Lohmann and Feichter, 2005; IPCC, 2007). Aerosols affect public health and are regulated as a priority air quality pollutant (Pope and Dockery, 2006; Chow et al., 2006). The Environmental Protection Agency (EPA), state and local governments monitor PM_{2.5} (particulate matter with diameter less than 2.5 μm) through surface monitoring networks, available to the public at the AIRNOW site (<http://airnow.gov>). To fill the gaps between the surface stations, satellite retrieved aerosol properties such as aerosol optical depth (AOD) have been used as a proxy to the surface PM_{2.5} (e.g. Al-Saadi et al., 2005; Hoff and Christopher, 2009; Zhang et al., 2009).

AOD retrievals from the polar-orbiting satellite instrument MODIS (Moderate-Resolution Imaging Spectroradiometer; Kaufman et al., 1997; Levy et al., 2007) provide a global daily coverage but sparse temporal sampling (once a day at mid-latitudes). Geostationary satellites offer high frequency observations resolving the diurnal cycle. This helps monitor significant events, such as wildfire smoke emissions, enable observation of prior aerosol motion, and potentially enable forecasting aerosol motion through data assimilation techniques. The GOES-East and GOES-West imagers observe the continental United States (CONUS) every half hour (Prados et al., 2007). The Spinning Enhanced Visible and Infrared Imager (SEVIRI) onboard the Meteosat Second Generation (MSG) satellite takes images of European-African area every 15 min (Popp et al., 2007). The current GOES imagers, however, have only a limited number of channels in the short wavelength part of the spectrum, and therefore a multi-channel algorithm like the one developed for MODIS cannot be applied to current GOES data. For the current GOES data, the GOES Aerosol/Smoke Product (GASP) was developed and has been operational at NOAA to monitor AOD over the United States (Knapp

AMTD

5, 7945–7981, 2012

GOES-East and GOES-West AOD retrieval

H. Zhang et al.

Title Page

Abstract

Introduction

Conclusions

References

Tables

Figures

⏪

⏩

◀

▶

Back

Close

Full Screen / Esc

Printer-friendly Version

Interactive Discussion



et al., 2002, 2005; Prados et al., 2007). A similar algorithm was also developed for SEVIRI in Europe (Popp et al., 2007).

GASP is applied independently to the two GOES satellites, GOES-East (currently GOES-13) at 75° W, and GOES-West (currently GOES-15) at 135° W. Figure 1 shows a schematic view of the solar-satellite geometries of the two satellites as a function of time during the day. The two GASP products are independent and at some times during the day with large scattering angles, the AOD retrievals for the two instruments can be quite different for the same surface location. In practice, the user is left to choose which geometry is likely to give the more precise result for their location. Prior work limited extreme viewing geometries so that the best retrieval is produced from the two algorithms, but even so there can be conflicting results. The quality assurance technique by which a combined answer from the two satellites is available is termed a “combined retrieval”. It should be possible, however, to use the additional information from the radiances and reflectances from the two satellites to add additional information, a “hybrid retrieval”, by giving additional degrees of freedom in the solution for AOD. This paper examines that option. It should be noted that to do so, the two satellites must be well inter-calibrated for reflectances and one spinoff from the current work is an additional satellite inter-calibration technique.

The most challenging task in the satellite AOD retrieval over land is separating the surface and aerosol contributions in the top of atmosphere (TOA) radiance. In order to have an AOD retrieval, the first step is to retrieve the surface reflectance. Unlike MODIS, which uses multichannel information to retrieve surface reflectance and AOD, the current GOES imagers have only one visible channel for aerosol and surface reflectance retrieval, which limits their retrieval accuracy. In the operational GASP algorithm (Knapp et al., 2002, 2005; Prados et al., 2007), a clear-sky composite background image is generated for each observation time by selecting the second darkest pixel of the images over the past 28 days. Surface reflectance is retrieved from the composite clear-sky image assuming that the background AOD is 0.02 for the clear-sky image. The assumption in the GASP algorithm is that the surface reflectance is constant at

**GOES-East and
GOES-West AOD
retrieval**

H. Zhang et al.

Title Page

Abstract

Introduction

Conclusions

References

Tables

Figures



Back

Close

Full Screen / Esc

Printer-friendly Version

Interactive Discussion



**GOES-East and
GOES-West AOD
retrieval**

H. Zhang et al.

[Title Page](#)[Abstract](#)[Introduction](#)[Conclusions](#)[References](#)[Tables](#)[Figures](#)[⏪](#)[⏩](#)[◀](#)[▶](#)[Back](#)[Close](#)[Full Screen / Esc](#)[Printer-friendly Version](#)[Interactive Discussion](#)

each observation time during the 28-day period. This algorithm works well when the assumption holds, which usually occurs in summer. However, surface reflectance can change rapidly due to the change of the solar position, the change of surface vegetation, and the change of the surface wetness during the 28-day period. Moreover, GASP can be affected by cloud shadows and underestimates the surface reflectance in the solar-satellite geometries where cloud shadows are often observed, e.g. in the afternoon over Western US.

To address this problem, Zhang et al. (2011) developed a new AOD retrieval algorithm for the GOES imager by adapting the Multi-Angle Implementation of Atmospheric Correction (MAIAC) algorithm originally developed for MODIS (Lyapustin and Wang, 2008; Lyapustin et al., 2011a,b). While this paper will not reproduce the entire MAIAC logic, a brief description is necessary to understand the new hybrid algorithm. GOES MAIAC assumes that the surface Bidirectional Reflectance Distribution Function (BRDF) in channel 1 of GOES is proportional to a seasonally averaged BRDF in the 2.1 μm MODIS channel. The coefficient of proportionality is derived through the time series analysis of the GOES visible channel images. This algorithm was shown to be more accurate than GASP over the Western US where the surface reflectance is usually high, i.e. greater than 0.15. However, this algorithm does not work well for backscattering view geometries (Fig. 1a for GOES-East or Fig. 1b for GOES-West), where the surface reflectance is much larger (the hotspot effect). The MODIS angular sampling usually is different from that of GOES, and as a result, the use of the MODIS BRDF shape gives large errors when the GOES view angles are close to the backscattering direction where BRDF varies the most.

Over the western third of the US, observations are available from both GOES-East and GOES-West imagers for much of the day. Since GOES-East and GOES-West observe the same region in different geometries, the TOA reflectance from the two satellites has different sensitivity to AOD. Such a feature can be exploited if observations from both satellites are used simultaneously. This adds one more degree of freedom to enable better retrieval of the surface reflectance. In this work, a new “hybrid” algorithm

GOES-East and GOES-West AOD retrieval

H. Zhang et al.

Title Page

Abstract

Introduction

Conclusions

References

Tables

Figures

⏪

⏩

◀

▶

Back

Close

Full Screen / Esc

Printer-friendly Version

Interactive Discussion



is developed that uses data from both satellites. It is found that morning observations from GOES-West (forward scattering directions) are more sensitive to AOD and less sensitive to surface reflectance than measurements from GOES-East (backscattering directions). Therefore, using a sensitivity parameter, the algorithm chooses GOES-West for AOD retrieval and GOES-East for the surface reflectance retrieval in the morning. In the afternoon, the view geometry and the retrieval strategy changes to the opposite satellite. The algorithm uses daily average AOD on clear days, when diurnal variability of AOD is expected to be low, to retrieve the BRDF shape. Section 2 of this paper describes the data used in this work. Section 3 gives a description of the AOD versus reflectance lookup procedure. Section 4 provides the detail of the algorithm. The algorithm validation based on AERONET data is described in Sects. 5 and 6 offers a new potential co-calibration philosophy for the two satellites.

2 Data sources

2.1 GOES imagers

Current GOES imagers have five channels, but only the visible channel can be used for aerosol retrieval. The current operational GOES-West is GOES-15, located above the equator at 135° W, so the satellite can view only the western third of the United States. GOES-15 replaced GOES-11 and started its operation in December, 2011. The current operational GOES-East is GOES-13. The previous GOES-East was GOES-12. GOES-12 stopped operation in April 2010 and was replaced by GOES-13. GOES-East is located at 75° W and it can view the whole continental US. For the hybrid algorithm to work, it is crucial that the two instruments be co-calibrated. The spectral response functions of the visible channel for the four satellite imagers relevant to this paper's study period are shown in Fig. 2 (data from ASPB and CIMSS Calibration Projects and Research, 2011). The differences of spectral response function (SRF) between GOES-11 and GOES-12 are small with the GOES-11 SRF slightly shifted towards red. Both

**GOES-East and
GOES-West AOD
retrieval**

H. Zhang et al.

[Title Page](#)[Abstract](#)[Introduction](#)[Conclusions](#)[References](#)[Tables](#)[Figures](#)[⏪](#)[⏩](#)[◀](#)[▶](#)[Back](#)[Close](#)[Full Screen / Esc](#)[Printer-friendly Version](#)[Interactive Discussion](#)

GOES-11 and GOES-12 visible channels cover the spectral range between 520 nm and 800 nm. The GOES-13 and GOES-15 SRFs are different from the other two and they have narrower spectral range, from 520 nm to 720 nm. Due to such difference, when switching from GOES-11 and GOES-12 pair to GOES-13 and GOES-15 pair in AOD retrieval algorithm, different look-up-tables should be generated.

Calibration for the GOES visible channel uses two calculations: one to get the calibrated on orbit radiance from the photon counts on the detector and the second to obtain the reflectance from the radiance (Weinreb et al., 1997). The radiance calibration between sensors has 1 % precision. In addition, the sensor calibration is allowed to change exponentially over time. In this work, calibration coefficients are obtained from the NOAA GOES Calibration site (NOAA GOES Calibration, 2011). As will be demonstrated below, the new hybrid algorithm involves solving for both AOD and reflectances simultaneously from the two satellites. This offers a new opportunity to co-calibrate these satellites. This will be discussed in Sect. 6, after the necessary explanation of the algorithm.

Prior to science processing, the image co-registration is applied to the GOES images to correct for jitter of the satellite orbit and correct the relatively low image navigation accuracy (4 km at nadir, GOES I-M databook, 1996). The procedure for co-registration of GOES-East image is the same as that described in (Zhang et al., 2011). The incoming images are compared with a predefined reference image at locations with high contrast using correlation analysis. The high contrast reference points are mostly located along the coastlines. The shift at each high contrast location is determined first. Then, the shift of each pixel is determined through linear regression. For the GOES-West image, we first re-project it to the GOES-East grid, and then apply the above procedure.

After the image co-registration using the control points along the coast lines, the GOES-West pixels may still not be co-located with those of GOES-East because these control points are not distributed evenly across GOES-West images. The coastline control points are mostly located in the middle of the image from north to south. To further improve the image co-location between the two satellites images, we use GOES-East

channel 1 image observed at the same time as the reference image and apply the same image co-registration algorithm on GOES-West image obtained at the same time as the reference image. The control points are selected such that they are evenly distributed over the whole image in cloud free conditions.

2.2 MODIS BRDF data

MODIS BRDF (Schaaf et al., 2002) in the 2.1 μm band is used as an aid for the retrieval of surface BRDF from GOES visible channel radiances in the MAIAC algorithm (Zhang et al., 2011).

The three Ross-Thick Li-Sparse (RTLS, Lucht et al., 2000) BRDF model parameters (k_{iso} , k_{geo} , k_{vol}) in the 2.1 μm band are obtained from the MODIS land products MCD43D19, MCD43D20, and MCD43D21 with a spatial resolution of 1 km. These BRDF parameters are derived from 16 days of MODIS surface reflectance (Vermote and Kotchenova, 2008) and are updated every eight days.

2.3 AERONET data

In the validation section below, the authors use the quality assured level 2.0 AERONET (AERosol RObotic NETwork, <http://aeronet.gsfc.nasa.gov>) AOD data for evaluating the AOD retrievals from GOES data. AERONET is a global ground aerosol monitoring network using CIMEL sunphotometers. The AERONET AOD is treated as ground-truth since the AERONET AOD data have an accuracy of ± 0.02 (Holben et al., 1998). Since AERONET AOD does not measure at wavelength 0.55 μm , it was calculated through log-linear interpolation between the two nearest wavelengths, i.e. 0.5 μm and 0.675 μm . Three sites from Western US are used in this study: UCSB (CA), Railroad Valley (NV) and Boulder (CO).

GOES-East and GOES-West AOD retrieval

H. Zhang et al.

Title Page

Abstract

Introduction

Conclusions

References

Tables

Figures

◀

▶

◀

▶

Back

Close

Full Screen / Esc

Printer-friendly Version

Interactive Discussion



3 Radiative transfer model and Look-Up-Table (LUT)

The retrieval algorithm for AOD is implemented with the aid of a look-up-table. The radiative transfer code SHARM (Lyapustin and Wang, 2005) is used to calculate TOA reflectance for different geometries, surface reflectance, and AOD. To retrieve the surface reflectance, the RTLS BRDF model is used as it is in MAIAC (Lyapustin et al., 2011a,b; Zhang et al., 2011) and in the MODIS BRDF/albedo product (Schaaf et al., 2002). This model includes an isotropic term, a volume-scattering term, and a geometric term (Roujean et al., 1992), and the BRDF is written as:

$$\rho_{\text{sfc}}(\theta_s, \theta_v, \Delta\phi) = k_{\text{iso}} + k_{\text{vol}}f_{\text{vol}}(\theta_s, \theta_v, \Delta\phi) + k_{\text{geo}}f_{\text{geo}}(\theta_s, \theta_v, \Delta\phi). \quad (1)$$

Here, k_{iso} , k_{vol} , and k_{geo} are the model parameters, f_{vol} and f_{geo} are pre-defined kernel functions depending only on the view geometry, defined by the triplet $(\theta_s, \theta_v, \Delta\phi)$ of the solar and view zenith angles and relative azimuth. Based on analysis of ground-based data as well as MODIS and POLDER measurements (Schaaf et al., 2002; Maignan et al., 2004), this model provides sufficient versatility and accuracy to describe bidirectional reflectance of natural surfaces. Based on the Green's function RT solution with anisotropic surface (Lyapustin and Knyazikhin, 2001), the TOA reflectance can approximately be written as (Lyapustin and Wang, 2008; Lyapustin et al., 2011a):

$$\rho_{\text{TOA}}(\theta_s, \theta_v, \Delta\phi) = \rho_D(\theta_s, \theta_v, \Delta\phi) + k_{\text{iso}}F_{\text{iso}}(\theta_s, \theta_v) + k_{\text{vol}}F_{\text{vol}}(\theta_s, \theta_v, \Delta\phi) + k_{\text{geo}}F_{\text{geo}}(\theta_s, \theta_v, \Delta\phi) \quad (2)$$

where ρ_D represents the atmospheric path reflectance, k_{iso} , k_{vol} , k_{geo} are RTLS coefficients defined in Eq. (1), F_{iso} , F_{vol} , F_{geo} are the integrals from the atmospheric upward and downward bidirectional transmittance multiplied by the isotropic, geometric and volumetric BRDF kernels, respectively. For the GOES visible channel, these functions depend on the aerosol properties (e.g. AOD) and geometry. The detailed expressions of can be found in Lyapustin and Wang (2008). Equation (2) also ignores a non-linear

Title Page

Abstract

Introduction

Conclusions

References

Tables

Figures

◀

▶

◀

▶

Back

Close

Full Screen / Esc

Printer-friendly Version

Interactive Discussion



term describing multiple scattering of photons between the surface and atmosphere, which is small for most surfaces.

An accurate accounting for anisotropic surface reflectance is important when the surface anisotropy and the diffuse surface irradiance are high, e.g. at shorter wavelengths, higher scattering optical depth and larger air mass (high zenith angles) (e.g. Wang et al., 2010). At the longer wavelength of the GOES visible channel compared to the 0.466 μm channel used in MODIS and the MODIS MAIAC algorithm, both Rayleigh and aerosol optical depth are lower in the GOES configuration. In this case, use of Lambertian assumption, which offers a much simpler mathematical model, gives an adequate accuracy as compared to other error sources. For example, Zhang et al. (2011) evaluated the GOES AOD retrieval uncertainty from the Lambertian assumption as less than 20 %. Therefore, in this study, a Lambertian model is used in the LUT calculation.

The LUT was generated using an aerosol model with fine and coarse fractions with lognormal size distribution and following (volumetric) parameters: radius $R_v = 0.14 \mu\text{m}$ and $3.2 \mu\text{m}$; standard deviation $\sigma_v = 0.35 \mu\text{m}$ and $0.7 \mu\text{m}$; real and imaginary part of index of refraction $n_r = 1.45$ and $n_i = 0.006$. The ratio of volumetric concentrations between the coarse and the fine mode is $C_{v,\text{coarse}}/C_{v,\text{fine}} = 0.5$. Fixed climatological values of column ozone and water vapor for gaseous absorption calculation are applied in the calculation of the LUT following (Knapp et al., 2002; Zhang et al., 2008).

4 Hybrid algorithm description

In the previous sections, the groundwork for understanding the hybrid algorithm is given. The GOES implementation of the MAIAC algorithm is used to get the range of surface reflectances for all scattering angles that the two satellites will see, i.e. the BRDF. Figure 3a and b shows the flow chart of the combined algorithm that uses both GOES-East and GOES-West data. Steps in the figure are identified by the corresponding section numbers in the text below.

GOES-East and GOES-West AOD retrieval

H. Zhang et al.

Title Page

Abstract

Introduction

Conclusions

References

Tables

Figures



Back

Close

Full Screen / Esc

Printer-friendly Version

Interactive Discussion



**GOES-East and
GOES-West AOD
retrieval**

H. Zhang et al.

[Title Page](#)[Abstract](#)[Introduction](#)[Conclusions](#)[References](#)[Tables](#)[Figures](#)[◀](#)[▶](#)[◀](#)[▶](#)[Back](#)[Close](#)[Full Screen / Esc](#)[Printer-friendly Version](#)[Interactive Discussion](#)

First, the cloud mask algorithm CLAVR (Clouds from Advanced Very High Resolution Radiometer; Stowe et al., 1999; Heidinger et al., 2001) is applied to detect cloudy pixels. CLAVR has been used in GOES-MAIAC (Zhang et al., 2011) and GASP (Prados et al., 2007) algorithms. It uses two IR channels 2 and 4, along with the visible channel.

5 While the visible channel 1 has spatial resolution of 1 km, it is the resolution of IR channels (4 km) that define spatial resolution of both cloud mask and AOD retrievals.

The GOES-MAIAC algorithm, which uses seasonally-averaged MODIS BRDF at 2.1 μm , works well over the Western US for the view geometries away from the backscattering direction where MODIS BRDF shape becomes inapplicable, namely for
10 the range of scattering angles $< 150\text{--}160^\circ$ (Zhang et al., 2011). In the new hybrid algorithm, the task is to obtain the correct BRDF for the full range of view angles. The new version of the algorithm expands GOES processing to cover the full range of GOES observations as follows.

4.1 AOD pre-screening for BRDF update

15 Armed with the knowledge of the BRDF from prior days, the first step is to determine whether the BRDF has changed due to meteorological (rain, snow, etc.) and vegetation factors. This assessment can only be done on clear days with low AOD impact. The morning data from GOES-West and the afternoon data from GOES-East, obtained in the forward scattering directions where the sensitivity of measurements to AOD is high,
20 are used to derive an AOD estimate using GOES-MAIAC algorithm. Since the aerosol horizontal scale is approximately 80 km (Anderson et al., 2003), a $100 \times 100 \text{ km}^2$ region is used to estimate the average AOD from MAIAC as a screening tool for clear days. This step utilizes a requirement that there be sensitivity to AOD in the change in reflectance (largely a scattering geometry constraint). That change in AOD versus
25 change in reflectance is determined from the MODIS BRDF and a forward calculation. A constraint that at least 40 % of the pixels in this region have AOD retrievals is also used to eliminate cloudy regions.

**GOES-East and
GOES-West AOD
retrieval**

H. Zhang et al.

Title Page

Abstract

Introduction

Conclusions

References

Tables

Figures

◀

▶

◀

▶

Back

Close

Full Screen / Esc

Printer-friendly Version

Interactive Discussion



Figure 4 shows the morning and afternoon solution curves of surface reflectivity and AOD for measured TOA reflectances from the two satellites at Boulder CO. In this figure, the surface reflectivity is scaled to the previous day's reflectivity (no change in reflectance is represented by unity on the abscissa). There is a range of values of this change for which unphysical solutions exist or for which the sensitivity to AOD is low (curves above the long dashed lines). This provides the criterion above for sensitivity between AOD and reflectance.

Analysis of diurnal cycle of AOD based on AERONET data was done previously (e.g. Smirnov et al., 2002). Among other results, this work showed low daily variability of AOD in clear conditions with low aerosol concentration. Here, an additional analysis is conducted based on a longer time series of AERONET measurements. Figure 5 shows the histogram of daily standard deviation of AOD at GSFC for the days with average AOD less than 0.3 using data from 1995 to 2008. One can see that the standard deviation of AOD is generally below 0.05, indicating that a daily average AOD (AOD^{av}) can be used to retrieve BRDF for low AOD days with sufficient accuracy.

The errors in AOD^{av} will propagate into BRDF retrievals and will affect the subsequent AOD retrievals. Assuming that AOD^{av} was overestimated by $\Delta\tau$, one can expect that this will lead to overestimation of AOD on the subsequent days (through BRDF-error) close to $\Delta\tau$. Figure 6 shows the result of such sensitivity study conducted for the surface reflectance 0.1 and over-estimation $\Delta\tau = 0.05$ of AOD^{av} for different daily AOD values. The overestimation of AOD on the subsequent days is found to be close to 0.05. The error is slightly larger at low AOD and becomes lower than 0.05 at larger AOD. Based on this consideration, the criterion $AOD < 0.3$ is found to be acceptable within that error to select clear days for the BRDF retrieval.

In the previous analysis of GOES-East data, Zhang et al. (2011) found that the GOES-MAIAC algorithm has a good AOD retrieval accuracy over the Western US in the afternoon, for the forward scattering geometries when surface BRDF is low and sensitivity of TOA reflectance to AOD is high. The GOES-West instrument samples similar view geometries (forward scattering) in the morning for the Western US. This

GOES-East and GOES-West AOD retrieval

H. Zhang et al.

Title Page

Abstract

Introduction

Conclusions

References

Tables

Figures

◀

▶

◀

▶

Back

Close

Full Screen / Esc

Printer-friendly Version

Interactive Discussion



is illustrated in Fig. 7 showing computed TOA reflectance as a function of UT time for different AOD values (0, 0.5, and 1.0) for Railroad Valley, Nevada, using BRDF typical for this location. One can see that GOES-West radiance has high sensitivity to AOD variations in the morning before 17:00 UT (the lines corresponding to different AODs in Fig. 7 are well separated), while the same is true for GOES-East in the afternoon after 21:00 UT, when both instruments sample the low part of surface BRDF in the forward scattering geometry. During the time between 17:00 and 21:00 UT, neither is sensitive to AOD due to relatively high surface reflectance. Based on the above discussion, the average AOD^{av} is obtained as an average from GOES-East AOD and GOES-West AOD retrieved from GOES-MAIAC at the observations with scattering angle less than 80°. The day is marked as clear (good for BRDF retrieval) if both AODs are below 0.3 and agree with each other to within 0.1 so that the AOD variation is estimated to be below 0.05. It is also required that the sensitivity measure $\Delta\tau/\Delta\rho_{\text{sfc}}$ is less than 0 and greater than -20 at the particular geometry and TOA reflectance (see Zhang et al., 2011). This represents the curves that are below the long dashed lines in Fig. 4. As AOD^{av} represents a large area, we require the cloud fraction to be less than 60% in this area in order to have sufficient statistical power.

4.2 Retrieve surface reflectance

Clear days are defined when both morning and afternoon AOD are similar and low (AOD < 0.3). On such days, typical diurnal variation of AOD is also small (e.g. Smirnov et al., 2002), and the effect of AOD on retrieved surface reflectance is also small and assumed constant. This average AOD^{av} is used to derive the BRDF shape from combined GOES-West and GOES-East data for the full range of GOES observation geometries including the backscattering direction.

The time series of one-three days of GOES channel 1 images is used to derive surface BRDF. Since the GOES imager makes an observation every half hour, there are about a hundred images during the three daytime intervals from both GOES imagers.

A set of filters is applied to the accumulated time series to reduce possible noise:

**GOES-East and
GOES-West AOD
retrieval**

H. Zhang et al.

[Title Page](#)[Abstract](#)[Introduction](#)[Conclusions](#)[References](#)[Tables](#)[Figures](#)[⏪](#)[⏩](#)[◀](#)[▶](#)[Back](#)[Close](#)[Full Screen / Esc](#)[Printer-friendly Version](#)[Interactive Discussion](#)

(1) Cosine of solar zenith angle should be larger than 0.3 (72°). Because the surface reflectance retrieved at high solar zenith angle is less accurate due to the increased sensitivity of TOA reflectance to the AOD variations, the observations with high solar zenith angle are removed in the BRDF retrieval.

(2) To further reduce interference from cloud, cloud shadow and large variations of AOD, a filter is applied to remove measurements with large variations in the accumulated time series. This filter assumes that surface BRDF is stable for the period of 1–3 days, and thus the previous surface BRDF can be used as reference ($BRDF^{Ref}$) to filter measurements producing large deviations from the reference value. The threshold for this test is set to the bigger of $0.4 BRDF^{Ref}$ and 0.04. On the other hand, to account for a seasonal or rapid surface change, this filter is not applied if more than 85 % of the new surface reflectance values are systematically higher or lower than the reference values.

(3) In addition, the surface reflectance sequence is sorted by scattering angle and it is assumed that the surface reflectance increases with scattering angle, which generally holds true based on analysis of both MODIS and GOES BRDF retrievals. The surface reflectance at a particular time should be within a range determined by the values in the sequence before and after it, and it is removed if falling outside that range. In the current implementation, the threshold for this filter is set to 0.03 or 30 % of the surface reflectance, whichever is larger.

4.3 BRDF update

After application of the filters, the BRDF is updated by fitting the sequence of the surface reflectances to the RTLS model described in Eq. (1) if the number of remaining measurements is larger than 12. If the number of new measurements is less than 12, the preexisting BRDF is assumed valid. In the real-time processing, the BRDF retrieval process is performed during the night when all the daytime GOES data are available. The updated BRDF is used on the following day together with the new incoming GOES data for the AOD retrieval.

4.4 AOD retrieval on current day data

The current surface BRDF is assumed proportional to the one updated in the previous step:

$$\rho_{\text{sfc}}(\theta_s, \theta_{vi}, \Delta\phi_i, \text{current}) = a\rho_{\text{sfc}}(\theta_s, \theta_{vi}, \Delta\phi_i, \text{previous}),$$

- 5 where $i = e, w$ represents two satellite geometries for GOES-East and GOES-West, respectively, and a represents a BRDF scaling factor. At any given time, there are two equations for the two GOES (-West and -East) measurements from Eq. (2):

$$\rho_{\text{TOA},i}(\tau, a) = \rho_{D,i}(\tau) + a(k_{\text{iso}}F_{\text{iso},i}(\tau) + k_{\text{geo}}F_{\text{geo},i} + k_{\text{vol}}F_{\text{vol},i}(\tau)),$$

10 where the definition geometry variables are fixed for a given observation time and are represented in the index i for the two satellites. The equations can be solved for two unknowns, a and AOD (τ). In many cases, this approach provides a reasonable solution while in other cases the retrieved values (a, τ) may have large uncertainty. Figure 4 demonstrates the two situations at two observation times at Boulder. The (a, τ) pairs on the GOES-East/GOES-West curves satisfy the measurement for the respective view
15 geometry, and the solution (a, τ) is represented by the intersection point. Although both cases have solutions, the case shown in Fig. 4b is strongly sensitive to the measurement uncertainties caused by the factors such as calibration, cloud contamination, etc. Thus, when slopes of the two curves are found close (as in Fig. 4b), we assume $a = 1$ and retrieve AOD using the sensor (-East or -West) that is more sensitive to AOD variations. AOD is retrieved for the current day and the coefficient for BRDF for the following
20 day is computed (Fig. 3b).

The quantity $S = \frac{\Delta\tau}{\Delta\rho_{\text{sfc}}}\rho_{\text{sfc}}$ computed at AOD = 0 for the corresponding geometry and TOA reflectance is used to differentiate the two situation in Fig. 4, since it is proportional to the reciprocal of the slopes of the curves. At a given observation time, S for GOES-East and GOES-West, i.e. S_e and S_w are calculated from LUT. If both S is less than
25 0 and greater than -2 , the slopes between the two curves are close (as in Fig. 4b)

GOES-East and GOES-West AOD retrieval

H. Zhang et al.

Title Page

Abstract

Introduction

Conclusions

References

Tables

Figures

◀

▶

◀

▶

Back

Close

Full Screen / Esc

Printer-friendly Version

Interactive Discussion



and thus we do not retrieve BRDF coefficient. In such situations, we assume the BRDF coefficient be 1 and retrieve AOD using the satellite data with larger S , which it is more sensitive to AOD variation. If the condition that both S is less than 0 and greater than -2 is not satisfied (as in Fig. 4a), surface reflectance coefficient a and AOD are solved simultaneously.

5 Results

5.1 Comparison to AERONET AOD

The AOD retrieval results are compared against the AERONET measurements at three AERONET sites located in the Western United States: Railroad Valley, UCSB, and Boulder. To find the coincidence between GOES AOD retrieval and AERONET measurements, we use the average GOES AOD retrievals within 5×5 box ($20 \times 20 \text{ km}^2$) surrounding the AERONET site and the interpolation of two closest AERONET measurements within 15 min before and after GOES observation. In cases where only one AERONET measurement is available within 15 min time frame, that value is used instead of interpolation. To further remove cloud contamination, it is required at least 10 retrievals among the 25 pixels and standard deviation of AOD in the 5×5 box less than 0.2. The combined algorithm only works when both satellites have observations at the same time. At some observation times, there are not data from both satellites, i.e. GOES-West does not have observations at 15:15, 15:45, 18:15, 21:15, and 21:45 UT. In this validation, the data for GOES-East is from GOES-12 and the data for GOES-West is from GOES-11. The time period of the data is from 1 March 2008 to 31 October 2008.

The single satellite algorithm was run on the three sites as well as the new hybrid algorithm and their results are compared. In Fig. 8, the results of validation of the hybrid algorithm are shown for western sites: UCSB, Railroad Valley and Boulder. In all the three sites, the number of retrievals has increased in the hybrid algorithm over

GOES-East and GOES-West AOD retrieval

H. Zhang et al.

Title Page

Abstract

Introduction

Conclusions

References

Tables

Figures



Back

Close

Full Screen / Esc

Printer-friendly Version

Interactive Discussion



GOES-East and GOES-West AOD retrieval

H. Zhang et al.

Title Page

Abstract

Introduction

Conclusions

References

Tables

Figures

⏪

⏩

◀

▶

Back

Close

Full Screen / Esc

Printer-friendly Version

Interactive Discussion



the individual satellite retrievals, by 5% to 80% for the three sites. At Boulder, the hybrid algorithm also improves the retrieval accuracy., The RMSE reduces to 0.06 for the hybrid algorithm compared to 0.09 for GOES-West and 0.10 for GOES-East. At the other two sites, the accuracy of the hybrid algorithm is similar to the single satellite algorithm. At UCSB, the surface reflectance is low in all the geometries, i.e. below 0.1 most of the time, the retrieval can be obtained from both satellites retrievals. Therefore, the number of the hybrid retrieval is similar to those of the single satellite retrievals. At the other two sites, the surface reflectances are higher and there are observation times when single satellite measurement is not sensitive enough to have good retrievals. Thus, the number of hybrid retrievals is much larger than the number of single satellite retrievals at these two sites.

This example demonstrates the complementary nature between GOES-West and GOES-East. For any single sensor over surface with high surface reflectance, there is an observation time period when AOD cannot be retrieved due to low sensitivity to aerosol variations (backscattering angles). The hybrid algorithm solves this problem because the other sensor has a view geometry, favorable for aerosol retrieval, for the same period.

A combined method can also be applied to merge the retrievals from the single satellite retrievals: the AOD retrievals are selected from the satellite that has smaller scatter angle. Smaller scatter angle implies smaller surface reflectance and better sensitivity to AOD variations. The results of the combined algorithm at the three sites are shown in the last column of Fig. 8. The number of retrievals of the combined algorithm is similar to that of the hybrid algorithm. The accuracy of the combined algorithm is also similar to the hybrid algorithm at UCSB and Railroad Valley. But it is less accurate than the hybrid algorithm at Boulder, although it has improved accuracy over single satellite retrieval. Figure 9 shows the diurnal variation of RMSE of AOD retrievals from the hybrid algorithm and the combined algorithm. The RMSEs are calculated for the co-incident data that are contained in the retrievals from both algorithms. At Boulder, the

hybrid algorithm has lower RMSE most of the time. At the other two sites, there are no significant differences between the two algorithms.

5.2 A regional AOD retrieval example

Figure 10 shows the AOD retrieval maps for a California fire case on 10 July 2008 at 16:45 UT and at 22:15 UT. The figure shows AOD retrievals from single satellite algorithm for GOES-West and GOES-East as well as AOD retrievals from the hybrid algorithm. At 16:45 UT (local morning), channel 1 observation from GOES-East corresponds to a large scattering angle and high surface reflectance when accurate aerosol retrieval is not possible. At the same time, the GOES-West observation for the same scene has more favorable geometry with low surface reflectance, and as a result, GOES-West gives much better AOD retrieval coverage as compared to GOES-East at 16:45 UT. The hybrid algorithm at 16:45 UT gives retrieval coverage similar to that of GOES-West since it primarily relies on GOES-West data which have good sensitivity to AOD. The situation is reversed at 22:15 UT (local afternoon) when GOES-East becomes the primary sensor for AOD retrievals and gives the better retrieval coverage. Thus, the hybrid algorithm maximizes the retrieval coverage/accuracy from individual sensors and provides the best diurnal coverage and accuracy.

6 Inter-calibration of channel 1 images between the two satellites

The joint use of GOES-West and GOES-East data implies their good relative calibration. In this work, GOES-11 for GOES-West and GOES-12 for GOES-East are used when they were both in operation for the cross-calibration analysis. To this end, the BRDF retrieved from GOES-West and GOES-East are compared at Boulder, Colorado in the period 1 March 2008 to 31 October 2008 in a $20 \times 20 \text{ km}^2$ area around the site. Boulder (105.006° W , 40° N) is located almost midway between the two satellites in terms of view geometry. Therefore, the retrieved BRDF from the two satellites

GOES-East and GOES-West AOD retrieval

H. Zhang et al.

Title Page

Abstract

Introduction

Conclusions

References

Tables

Figures

◀

▶

◀

▶

Back

Close

Full Screen / Esc

Printer-friendly Version

Interactive Discussion



GOES-East and GOES-West AOD retrieval

H. Zhang et al.

Title Page

Abstract

Introduction

Conclusions

References

Tables

Figures

◀

▶

◀

▶

Back

Close

Full Screen / Esc

Printer-friendly Version

Interactive Discussion



are expected to be symmetric about local noon (19:00 UT). The BRDF retrieval algorithm described in Sect. 4 was applied separately for single satellite so that the BRDF was derived for each satellite. Analysis showed that the derived BRDF changes little if AOD from AERONET was used for each time step. Next, the surface reflectance from GOES-West was compared against that from GOES-East if it is mirrored at 19:00 UT. For example, the surface reflectance for GOES-West geometry at 18:00 UT should be the same as the surface reflectance for GOES-East geometry at 20:00 UT. Figure 11a shows the scatter plot of mirrored GOES-West vs. GOES-East surface reflectance retrievals. The surface reflectance from the two satellites are well correlated with $R = 0.99$. The GOES-West surface reflectance is a little higher than that of GOES-East with a slope of 1.08. By trial and error, application of a gain factor of 0.95 to GOES-West TOA reflectance was found to correct the slope between the two retrieved BRDFs to 1.0, as shown in Fig. 11b. Therefore, to make use of GOES-West and GOES-East channel 1 radiances in the hybrid algorithm, a gain factor of 0.95 was applied to GOES-West TOA reflectance data.

One potential error source in this analysis is a small eastward slope about 0.22° in the area around Boulder AERONET site. The related uncertainty was estimated through perturbing the solar zenith angle and view zenith angle, calculating the perturbed surface reflectance using the retrieved BRDF, and comparing it with the original surface reflectance. This analysis showed that the uncertainty due to the slope of the surface is around 0.5%, an order of magnitude less than the difference between GOES-West and GOES-East found above. Therefore, a small surface slope over the Boulder area does not introduce noticeable errors in the inter-calibration between the two satellites.

An alternative method can also be applied to inter-calibrate the two satellites' channel 1 radiances. In this method, BRDF was retrieved first using daily average AOD obtained from GOES-MAIAC algorithm using GOES-East data, the same way as described above. Then, TOA reflectance in GOES-West geometry was calculated using the retrieved BRDF and daily average AOD. Last, the calculated and the measured TOA reflectance in GOES-West geometry was compared against each other. Figure 12

GOES-East and GOES-West AOD retrieval

H. Zhang et al.

Title Page

Abstract

Introduction

Conclusions

References

Tables

Figures

◀

▶

◀

▶

Back

Close

Full Screen / Esc

Printer-friendly Version

Interactive Discussion



shows the scatter plot between the calculated TOA reflectance and GOES-West TOA reflectance. In this figure, several outliers have been removed, which are apparently due to the cloud/cloud shadow contaminations. The linear regression relation between them is $\rho_{\text{cal}} = 0.95\rho_{\text{GOES-West}}$, where the regression intercept is forced to be 0 as the calculated TOA reflectance is expected to be 0 when GOES-West TOA reflectance is 0. Therefore, both of the two inter-calibration methods provide the same result.

Similar inter-calibration between visible channels of the two GOES imagers was done by Nguyen et al. (2004). They compared the reflectance observed from the two imagers along the 105°W line at noon assuming the two satellites observed the same TOA reflectance at that time. The methods provided in this work can be used as alternative ways for inter-calibrating GOES-East and GOES-West.

7 Conclusions

In this study, a new “hybrid” AOD retrieval algorithm was developed over the Western US utilizing both GOES-West and GOES-East satellite data. As far as the authors are aware, this is the first hybrid algorithm to use two satellites to retrieve AOD over a single location at a single time. In the new algorithm, daily average AOD in clear days with AOD less than 0.3 is used to derive surface BRDF. The algorithm is based on two assumptions: AOD variation is small during days with small daily average AOD; surface BRDF shape is relative stable and does not change much from day to day during short time intervals. Daily average AOD is derived from spatial and temporal averaging of the GOES-MAIAC AOD at geometries with good retrievals. With BRDF known, and when both sensors observe the same area, the algorithm selects either GOES-East or GOES-West data with higher sensitivity for AOD retrieval. The sensitivity is related to the surface brightness, and is generally high for the forward scattering geometries and poor at backscattering angles. The complementary nature of GOES-East and GOES-West is used in this work to cross-calibrate the two sensors based on surface BRDF or TOA reflectance data. The algorithm is validated at three AERONET sites and the

results compare well to the AERONET AOD with correlation coefficients of 0.67–0.81 and the RMSEs of 0.06–0.07. The use of both satellites significantly improves the AOD retrieval data coverage. Over the three sites, we observe improvement from 5 % to 80 % in number of coincidences with AERONET AOD. Such improvement in AOD retrieval coverage is also demonstrated in a regional retrieval example for California fire case in 2008.

Acknowledgements. This work is supported by GOES-R risk reduction program project # NA11NES4400005. The authors would like to thank Yujie Wang for discussions and suggestions on the inter-calibration of GOES-West and GOES-East.

References

- Al-Saadi, J., Szykman, J., Pierce, R. B., Kittaka, C., Neil, D., Chu, D. A., Remer, L., Gumley, L., Prins, E., Weinstock, L., MacDonald, C., Wayland, R., Dimmick, F., and Fishman, J.: Improving national air quality forecasts with satellite aerosol observations, *B. Am. Meteorol. Soc.*, 86, 1249–1261, doi:10.1175/BAMS-86-9-1249, 2005. 7947
- Anderson, T. L., Charlson, R. J., Winker, D. M., Ogren, J. A., and Holmen, K.: Mesoscale variations of tropospheric aerosols, *J. Atmos. Sci.*, 60, 119–136, 2003. 7955
- ASPB and CIMSS Calibration Projects and Research, available at: <http://cimss.ssec.wisc.edu/goes/calibration/> (last access: 1 December 2011), 2011. 7950
- Charlson, R. J., Schwartz, S. E., Hales, J. M., Cess, R. D., Coakley, J. A., Hansen, J. E., and Hoffman, D. J.: Climate forcing by anthropogenesis aerosols, *Science*, 255, 423–430, 1992. 7947
- Chow, J. C., Watson, J. G., Mauderly, J. L., Costa, D. L., Wyzga, R. E., Vedal, S., Hidy, G. M., Altshuler, S. L., Marrack, D., Heuss, J. M., Wolff, G. T., Pope III, C. A., and Dockery, D. W.: Health effects of fine particulate air pollution: lines that connect, critical review discussion, *J. Air Waste Manage.*, 56, 1368–1380, 2006. 7947
- GOES I-M databook, available at: <http://goes.gsfc.nasa.gov/text/goes.databook.html> (last access: 9 June 2009), 1996. 7951
- Heidinger, A. K., Anne, V. R., and Dean, C.: Using MODIS to estimate cloud contamination of the AVHRR data record, *J. Atmos. Ocean. Tech.*, 19, 586–601, 2001. 7955

GOES-East and GOES-West AOD retrieval

H. Zhang et al.

Title Page

Abstract

Introduction

Conclusions

References

Tables

Figures



Back

Close

Full Screen / Esc

Printer-friendly Version

Interactive Discussion



GOES-East and GOES-West AOD retrieval

H. Zhang et al.

Title Page

Abstract

Introduction

Conclusions

References

Tables

Figures

◀

▶

◀

▶

Back

Close

Full Screen / Esc

Printer-friendly Version

Interactive Discussion



- Hoff, R. and Christopher, S. A.: Remote sensing of particulate matter air pollution from space: have we reached the promised land, *J. Air Waste Manage.*, 59, 642–675, 2009. 7947
- Holben, B. N., Eck, T. F., Slutsker, I., Tanr, D., Buis, J. P., Setzer, A., Vermote, E., Reagan, J. A., Kaufman, Y. J., Nakajima, T., Lavenu, F., Jankowiak, I., and Smirnov, A.: AERONET: a federated instrument network and data archive for aerosol characterization, *Remote Sens. Environ.*, 66, 1–16, 1998. 7952
- Intergovernmental Panel on Climate Change: Climate Change 2007, The Physical Science Basis, Cambridge Univ. Press, Cambridge, UK, 2007. 7947
- Kaufman, Y. J., Tanr, D., Remer, L. A. Vermote, E., Chu, A., and Holben, B. N.: Operational remote sensing of tropospheric aerosol over land from EOS moderate resolution imaging spectroradiometer, *J. Geophys. Res.*, 102, 17051–17067, 1997. 7947
- Kiehl, J. T. and Briegleb, B. P.: The radiative roles of sulfate aerosols and greenhouse gases in climate forcing, *Science*, 260, 311–314, 1993. 7947
- Knapp, K. R., Vonder Haar, T. H., and Kaufman, Y. J.: Aerosol optical depth retrieval from GOES-8: uncertainty study and retrieval validation over South America, *J. Geophys. Res.*, 107, 4055, doi:10.1029/2001JD000505, 2002. 7947, 7948, 7954
- Knapp, K. R., Frouin, F., Kondragunta, S., and Prados, A. I.: Towards aerosol optical depth retrievals over land from GOES visible radiances: determining surface reflectance, *Int. J. Remote Sens.*, 26, 4097–4116, 2005. 7948
- Levy, R. C., Remer, L. A., Mattoo, S., Vermote, E., and Kaufman, Y. J.: Second-generation operational algorithm: retrieval of aerosol properties over land from inversion of moderate resolution imaging spectroradiometer spectral reflectance, *J. Geophys. Res.*, 112, 13211, doi:10.1029/2006JD007811, 2007. 7947
- Li, X. and Strahler, A. H.: Geometric-optical bidirectional reflectance modeling of the discrete crown vegetation canopy: effect of crown shape and mutual shadowing, *IEEE T. Geosci. Remote*, 30, 276–292, 1992.
- Lohmann, U. and Feichter, J.: Global indirect aerosol effects: a review, *Atmos. Chem. Phys.*, 5, 715–737, doi:10.5194/acp-5-715-2005, 2005. 7947
- Lucht, W., Schaaf, C. B., and Strahler, A. H.: An Algorithm for the retrieval of albedo from space using semiempirical BRDF models, *IEEE T. Geosci. Remote*, 38, 977–998, 2000. 7952
- Lyapustin, A. and Knyazikhin, Y.: Greens function method in the radiative transfer problem. I: Homogeneous non-lambertian surface, *Appl. Optics*, 50, 3495–3501, 2001. 7953

GOES-East and GOES-West AOD retrieval

H. Zhang et al.

Title Page

Abstract

Introduction

Conclusions

References

Tables

Figures

◀

▶

◀

▶

Back

Close

Full Screen / Esc

Printer-friendly Version

Interactive Discussion



- Lyapustin, A. and Wang, Y.: Parameterized code Sharm-3-D for radiative transfer over inhomogeneous surfaces, *Appl. Optics*, 55, 7602–7610, 2005. 7953
- Lyapustin, A. and Wang, Y.: MAIAC: Multi-Angle Implementation of Atmospheric Correction for MODIS, Algorithm Theoretical Basis Document (ver. 1.0), 2008. 7949, 7953
- 5 Lyapustin, A., Martonchik, J., Wang, Y., Laszlo, I., and Korokin, S.: Multiangle implementation of atmospheric correction (MAIAC): 1. Radiative transfer basis and look-up tables, *J. Geophys. Res.*, 116, 03210, doi:10.1029/2010JD014985, 2011a. 7949, 7953
- Lyapustin, A., Wang, Y., Laszlo, I., Kahn, R., Korokin, S., Remer, L., Levy, R., and Reid, J. S.: Multiangle implementation of atmospheric correction (MAIAC): 2. Aerosol algorithm, *J. Geophys. Res.*, 116, 03211, doi:10.1029/2010JD014986, 2011b. 7949, 7953
- 10 Maignan, F., Bron, F.-M., and Lacaze, R.: Bidirectional reflectance of Earth targets: evaluation of analytical models using a large set of spaceborne measurements with emphasis on the hot spot, *Remote Sens. Environ.*, 90, 210–220, 2004. 7953
- Martins, J. V., Tanré, D., Remer, L., Kaufman, Y., Mattoo, S. and Levy, R.: MODIS Cloud screening for remote sensing of aerosols over oceans using spatial variability, *Geophys. Res. Lett.*, 29, 8009, doi:10.1029/2001GL013252, 2002.
- 15 Nguyen, L., Doelling, D. R., Minnis, P., and Ayers, J. K.: Rapid technique to cross-calibrate satellite imager with visible channels, in: *EarthObserving Systems IX*, edited by: Barnes, W. L. and Butler, J. J., International Society for Optical Engineering SPIE Proceedings, 5542, 227–235, 2004. 7964
- NOAA: GOES Calibration site, available at: http://www.star.nesdis.noaa.gov/smcd/spb/fwu/homepage/GOES_star_cal.php (last access: 1 December 2011), 2011. 7951
- Pope III, C. A. and Dockery, D. W.: Health effects of fine particulate air pollution: lines that connect, critical review, *J. Air Waste Manage.*, 56, 709–742, 2006. 7947
- 25 Popp, C., Hauser, A., Foppa, N., and Wunderle, S.: Remote sensing of aerosol optical depth over Central Europe from MSG-SEVIRI data and accuracy assessment with ground-based AERONET measurements, 112, D24S11, doi:10.1029/2007JD008423, 2007. 7947, 7948
- Prados, A. I., Kondragunta, S., Ciren, P., and Knapp, K. R.: GOES Aerosol/Smoke Product (GASP) over North America: comparisons to AERONET and MODIS observations, *J. Geophys. Res.*, 112, 15201, doi:10.1029/2006JD007968, 2007. 7947, 7948, 7955
- 30 Ramanathan, V., Crutzen, P. J., Kiehl, J. T., and Rosenfeld, D.: Aerosols, climate and the hydrological cycle, *Science*, 294, 2119–2124, 2001. 7947

GOES-East and GOES-West AOD retrieval

H. Zhang et al.

[Title Page](#)[Abstract](#)[Introduction](#)[Conclusions](#)[References](#)[Tables](#)[Figures](#)[◀](#)[▶](#)[◀](#)[▶](#)[Back](#)[Close](#)[Full Screen / Esc](#)[Printer-friendly Version](#)[Interactive Discussion](#)

Ross, J. K.: The Radiation Regime and Architecture of Plant Stands, edited by: Junk, W., Norwell, MA, Artech House, 392 pp., 1981.

Roujean, J. L., Leroy, M., and Deschamps, P. Y.: A bidirectional reflectance model of the Earth's surface for the correction of remote sensing data, *J. Geophys. Res.*, 97, 20455–20468, 1992. 7953

Schaaf, C. B., Gao, F., Strahler, A. H., Lucht, W., Li, X., Tsang, T., Strugnell, N. C., Zhang, X., Jin, Y., Muller, J.-P., Lewis, P., Barnsley, M., Hobson, P., Disney, M., Roberts, G., Dunderdale, M., Doll, C., d'Entremont, R., Hu, B., Liang, S., and Privette, J. L.: First operational BRDF, albedo and nadir reflectance products from MODIS, *Remote Sens. Environ.*, 83, 135–148, 2002. 7952, 7953

Schmit, T. J., Li, J., Gurka, J. J., Goldberg, M. D., Schrab, K. J., Li, J., and Feltz, W. F.: The GOES-R advanced baseline imager and the continuation of current sounder products, *J. Appl. Meteorol. Clim.*, 47, 2696–2711, doi:10.1175/2008JAMC1858.1, 2008.

Smirnov, A., Holben, B. N., Eck, T. F., Slutsker, I., Chatenet, B., and Pinker, R. T.: Diurnal variability of aerosol optical depth observed at AERONET (Aerosol Robotic Network) sites, *Geophys. Res. Lett.*, 29, 2115, doi:10.1029/2002GL016305, 2002. 7956, 7957

Stowe, L. L., Davis, P. A., and McClain, E. P.: Scientific basis and initial evaluation of CLAVR-1 global clear/cloud classification algorithm for the advanced very high resolution radiometer, *J. Atmos. Ocean. Tech.*, 16, 656–681, 1999. 7955

Vermote, E. F. and Kotchenova, S.: Atmospheric correction for the monitoring of land surfaces, *J. Geophys. Res.*, 113, D23S90, doi:10.1029/2007JD009662, 2008. 7952

Weinreb, M. P., Jamison, M., Fulton, N., Chen, Y., Johnson, J. X., Bremer, J., Smith, C., and Baucom, J.: Operational calibration of geostationary operational environmental satellite-8 and -9 imagers and sounders, *Appl. Optics*, 36, 6895–6904, 1997. 7951

Wang, Y., Lyapustin, A., Privette, J., Cook, R., SanthanaVannan, S. K., Vermote, E., and Schaaf, C.: Assessment of biases in MODIS surface reflectance due to Lambertian approximation, *Remote Sens. Environ.*, 114, 2791–2801, doi:10.1016/j.rse.2010.06.013, 2010. 7954

Wanner, W., Li, X., and Strahler, A. H.: On the derivation of kernels for kernel-driven models of bidirectional reflectance, *J. Geophys. Res.*, 100, 21077–21090, 1995.

Zhang, H., Hoff, R. M., McCann, K., Ciren, P., Kondragunta, S., and Prados, A.: Influence of the ozone and water vapor on the GOES Aerosol and Smoke Product (GASP) retrieval, NOAA Technical report NESDIS 128, 2008. 7954

Zhang, H., Hoff, R. M., and Kondragunta, S.: Development of IDEA product for GOES-R aerosol data, Proc. SPIE, 7456, 74560O, doi:10.1117/12.828095, 2009. 7947

Zhang, H., Lyapustin, A., Wang, Y., Kondragunta, S., Laszlo, I., Ciren, P., and Hoff, R. M.: A multi-angle aerosol optical depth retrieval algorithm for geostationary satellite data over the United States, Atmos. Chem. Phys., 11, 11977–11991, doi:10.5194/acp-11-11977-2011, 2011. 7949, 7951, 7952, 7953, 7954, 7955, 7956, 7957

5

AMTD

5, 7945–7981, 2012

GOES-East and GOES-West AOD retrieval

H. Zhang et al.

Title Page

Abstract

Introduction

Conclusions

References

Tables

Figures

⏪

⏩

◀

▶

Back

Close

Full Screen / Esc

Printer-friendly Version

Interactive Discussion



GOES-East and GOES-West AOD retrieval

H. Zhang et al.

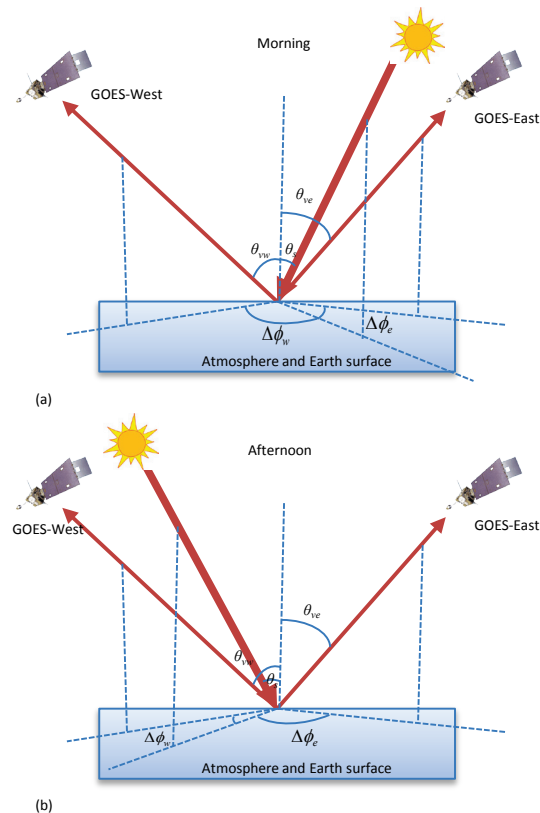


Fig. 1. The scattering geometry of the Sun and the two GOES satellites **(a)** in the morning and **(b)** in the afternoon for Western US region. The angles in the figure are defined as following: θ_s – solar zenith angle, θ_{vw} – GOES-West view zenith angle, θ_{ve} – GOES-East view zenith angle, $\Delta\phi_w$ – relative azimuth angle between the Sun and GOES-West, $\Delta\phi_e$ – relative azimuth angle between the Sun and GOES-East.

[Title Page](#)
[Abstract](#)
[Introduction](#)
[Conclusions](#)
[References](#)
[Tables](#)
[Figures](#)
[Back](#)
[Close](#)
[Full Screen / Esc](#)
[Printer-friendly Version](#)
[Interactive Discussion](#)


**GOES-East and
GOES-West AOD
retrieval**

H. Zhang et al.

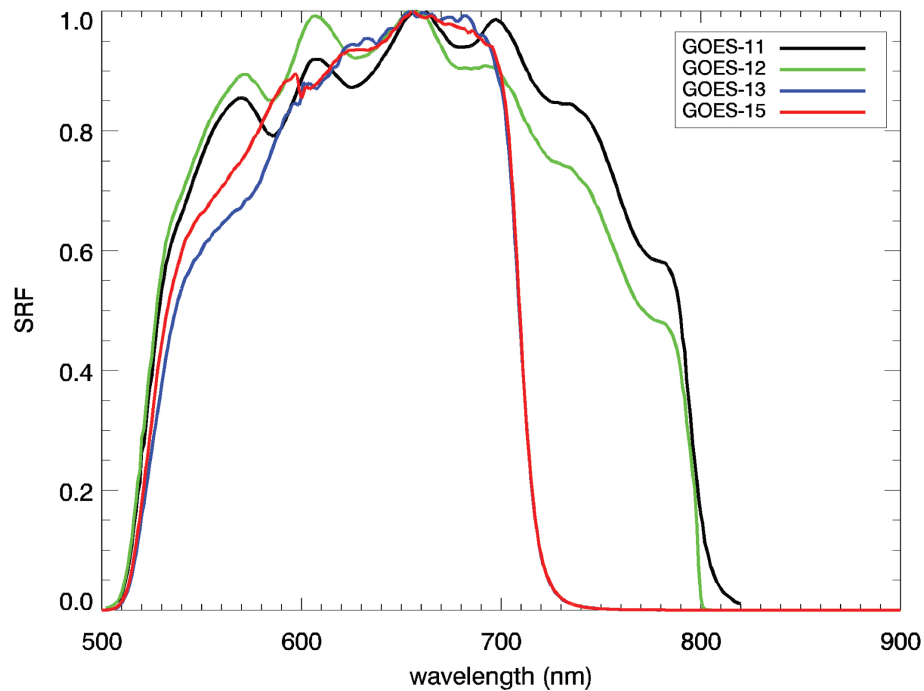


Fig. 2. Spectral response functions of the visible channels of the four GOES satellites (ASPB and CIMSS Calibration Projects and Research, 2011).

[Title Page](#)[Abstract](#)[Introduction](#)[Conclusions](#)[References](#)[Tables](#)[Figures](#)[◀](#)[▶](#)[◀](#)[▶](#)[Back](#)[Close](#)[Full Screen / Esc](#)[Printer-friendly Version](#)[Interactive Discussion](#)

GOES-East and GOES-West AOD retrieval

H. Zhang et al.

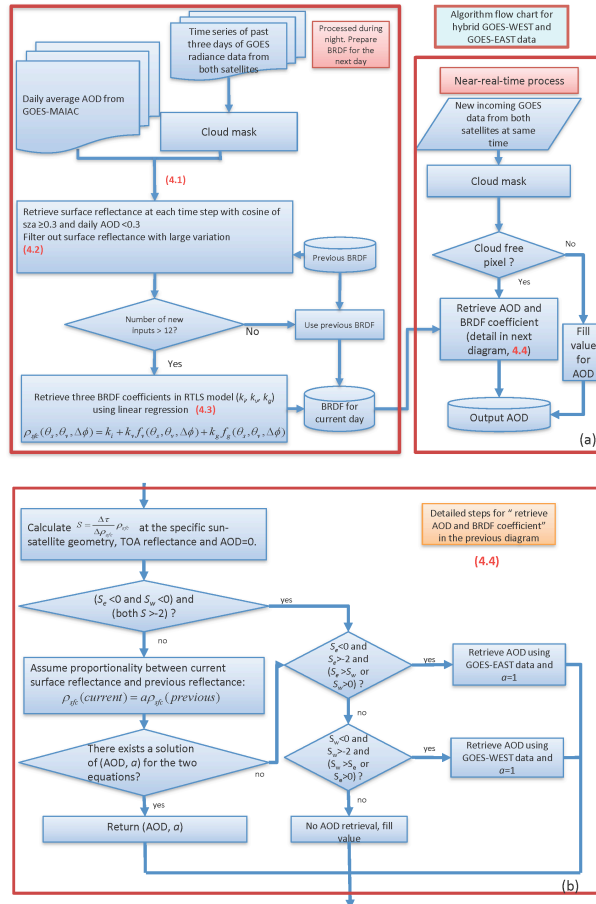


Fig. 3. (a) Flow chart. Section number descriptions in the text are noted to help follow the flow of the hybrid AOD and BRDF retrieval algorithm. (b) Detailed steps for AOD and BRDF coefficient retrieval in (a).

Title Page

Abstract Introduction

Conclusions References

Tables Figures

◀ ▶

◀ ▶

Back Close

Full Screen / Esc

Printer-friendly Version

Interactive Discussion

GOES-East and GOES-West AOD retrieval

H. Zhang et al.

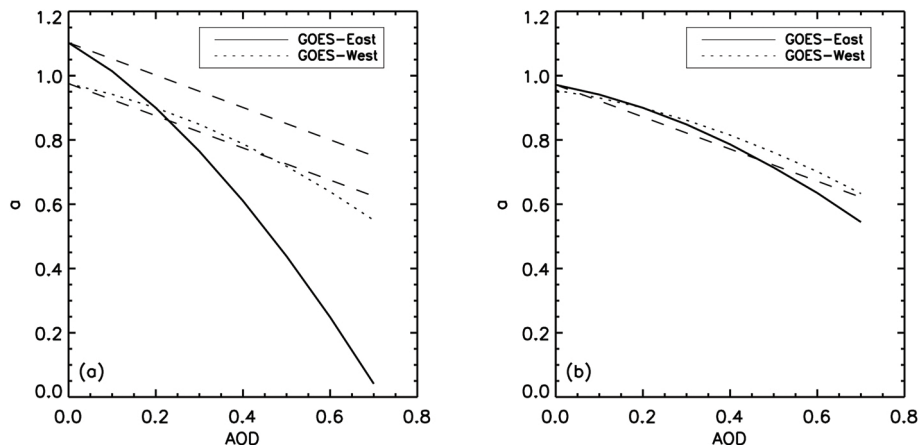


Fig. 4. AOD and surface reflectance solution curve for two satellites geometries at Boulder **(a)** 22:00 UT and **(b)** 20:00 UT, where ρ represents surface reflectance normalized by the previous day surface reflectance. The TOA reflectance was calculated using $a = 0.9$ and $AOD = 0.2$. If a solution curve is above the long dashed line, i.e. the absolute value of the slope of the curve is less than that of the dashed line, the TOA reflectance is not sensitive to the AOD variations, and vice versa.

[Title Page](#)
[Abstract](#)
[Introduction](#)
[Conclusions](#)
[References](#)
[Tables](#)
[Figures](#)
[◀](#)
[▶](#)
[◀](#)
[▶](#)
[Back](#)
[Close](#)
[Full Screen / Esc](#)
[Printer-friendly Version](#)
[Interactive Discussion](#)


GOES-East and GOES-West AOD retrieval

H. Zhang et al.

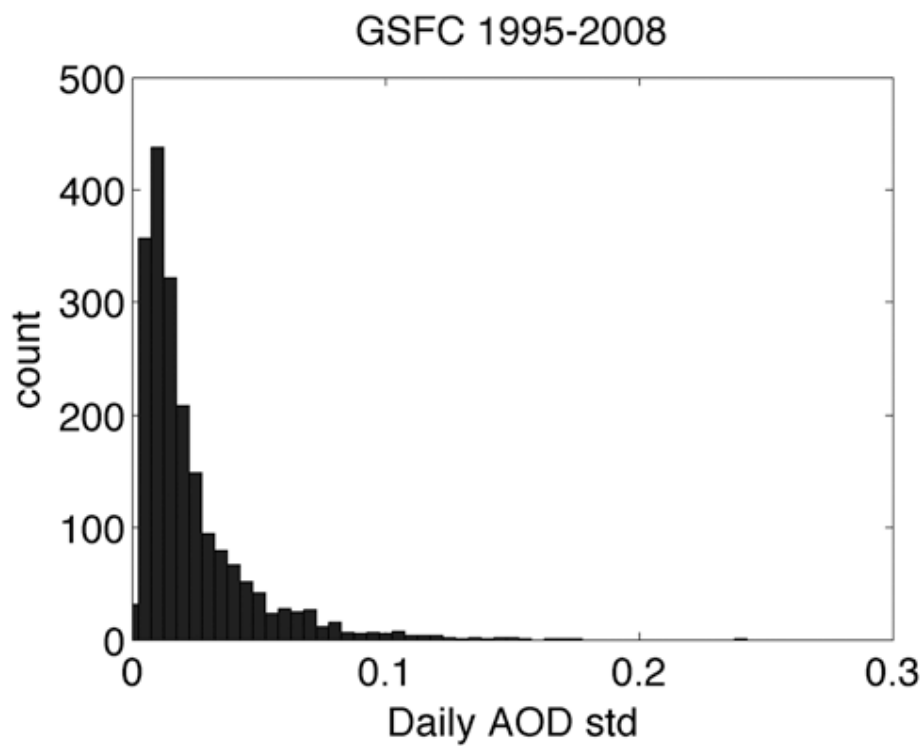


Fig. 5. Histogram of daily standard deviation of AOD with average values less than 0.3 at GSFC AERONET site from 1995 to 2008.

Title Page

Abstract

Introduction

Conclusions

References

Tables

Figures

◀

▶

◀

▶

Back

Close

Full Screen / Esc

Printer-friendly Version

Interactive Discussion



GOES-East and GOES-West AOD retrieval

H. Zhang et al.

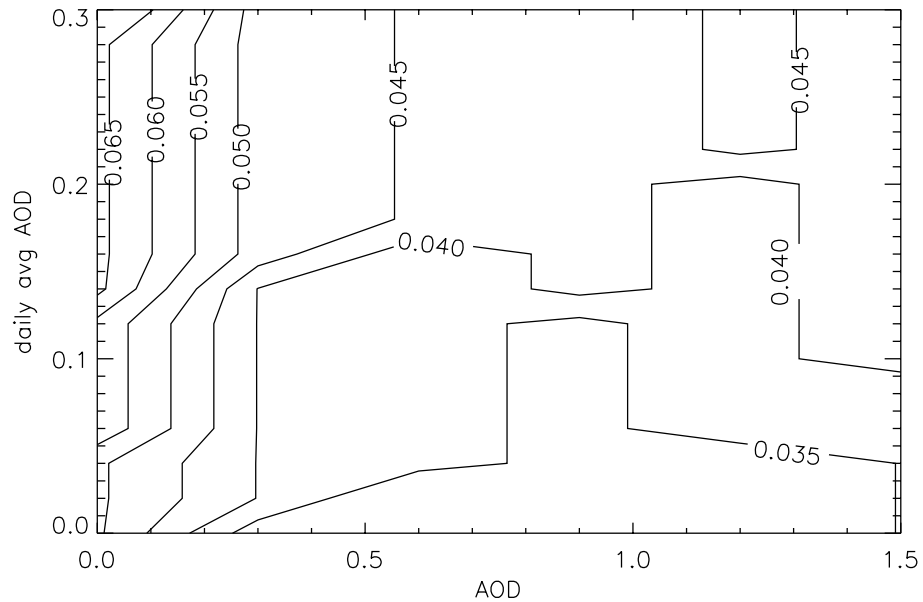


Fig. 6. Sensitivity of AOD retrieval to the errors in daily average AOD. The geometry is set for GOES-East at Railroad Valley on day 213 at 22:00 UT with surface reflectance assumed to be 0.1.

Title Page

Abstract

Introduction

Conclusions

References

Tables

Figures

⏪

⏩

◀

▶

Back

Close

Full Screen / Esc

Printer-friendly Version

Interactive Discussion



GOES-East and GOES-West AOD retrieval

H. Zhang et al.

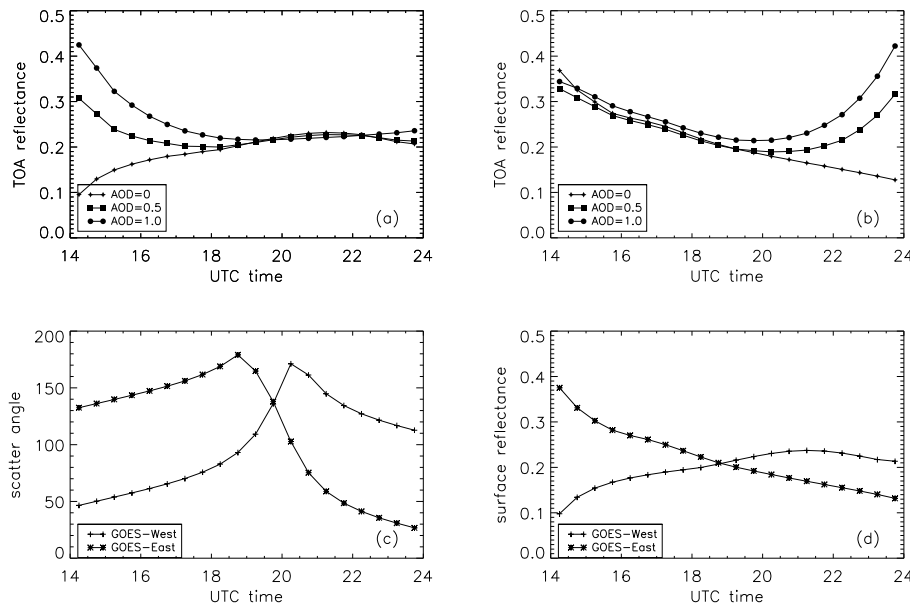


Fig. 7. TOA reflectance vs. UT time calculated in the (a) GOES-West and (b) GOES-East geometry for Railroad Valley. The radiative transfer model, aerosol model and gases absorption parameters used are the same as those for look-up-table in Sect. 3. (c) Scatter angle viewed from GOES-West and GOES-East during the time in (a) and (b). (d) Surface reflectance in the GOES-West and GOES-East geometries vs. UT time.

Title Page

Abstract

Introduction

Conclusions

References

Tables

Figures

◀

▶

◀

▶

Back

Close

Full Screen / Esc

Printer-friendly Version

Interactive Discussion



GOES-East and GOES-West AOD retrieval

H. Zhang et al.

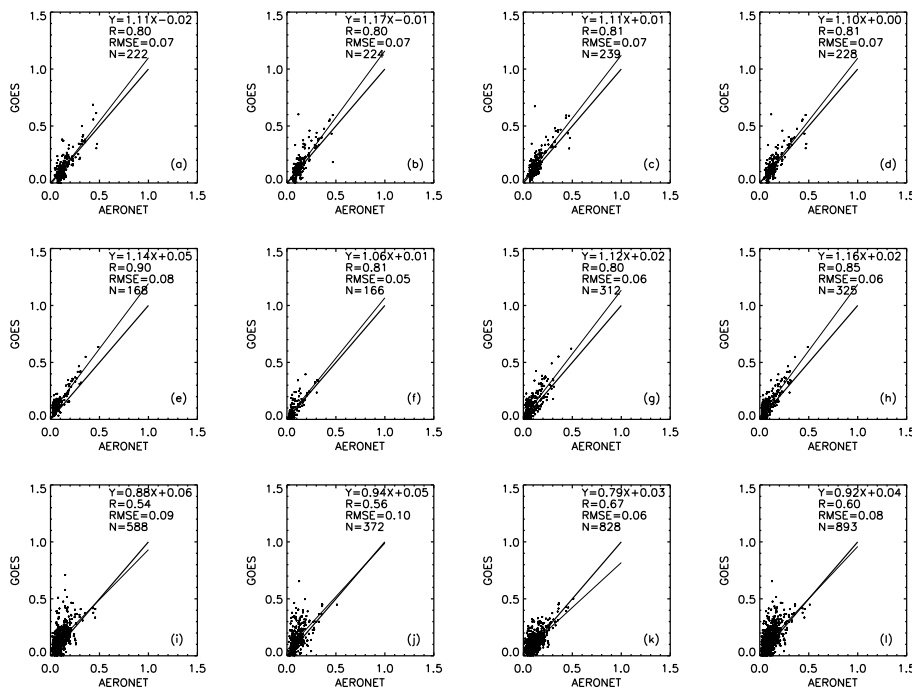


Fig. 8. Scatter plots of AOD for GOES-WEST vs. AERONET (column 1), GOES-EAST vs. AERONET (column 2), hybrid algorithm vs. AERONET (column 3), and combined algorithm (column 4) at three AERONET site: UCSB (top row), Railroad Valley (middle row), and Boulder (bottom row).

[Title Page](#)
[Abstract](#)
[Introduction](#)
[Conclusions](#)
[References](#)
[Tables](#)
[Figures](#)
[Back](#)
[Close](#)
[Full Screen / Esc](#)
[Printer-friendly Version](#)
[Interactive Discussion](#)


GOES-East and GOES-West AOD retrieval

H. Zhang et al.

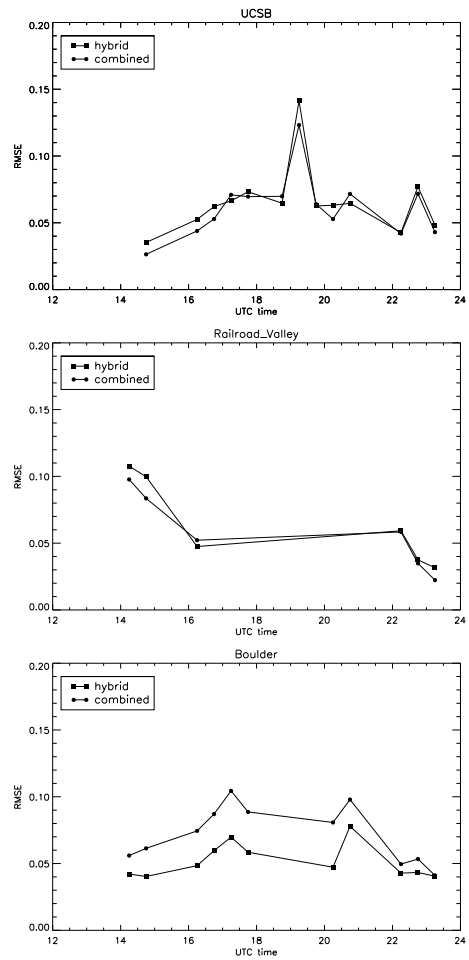


Fig. 9. Diurnal variation of RMSE of GOES AOD retrievals for the hybrid algorithm and the combined algorithm.

[Title Page](#)
[Abstract](#) [Introduction](#)
[Conclusions](#) [References](#)
[Tables](#) [Figures](#)
[◀](#) [▶](#)
[◀](#) [▶](#)
[Back](#) [Close](#)
[Full Screen / Esc](#)
[Printer-friendly Version](#)
[Interactive Discussion](#)



GOES-East and GOES-West AOD retrieval

H. Zhang et al.

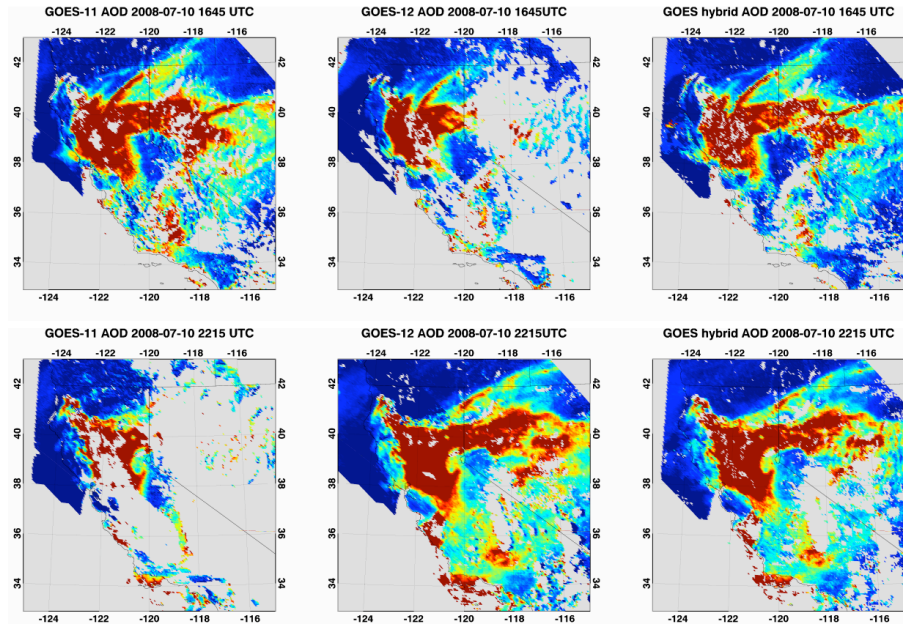


Fig. 10. Comparison of AOD retrievals from single satellite algorithm and from the hybrid algorithm for California fire case on 10 July 2008 at two observation times: 16:45 UT and 22:15 UT.

Title Page

Abstract

Introduction

Conclusions

References

Tables

Figures

◀

▶

◀

▶

Back

Close

Full Screen / Esc

Printer-friendly Version

Interactive Discussion



**GOES-East and
GOES-West AOD
retrieval**

H. Zhang et al.

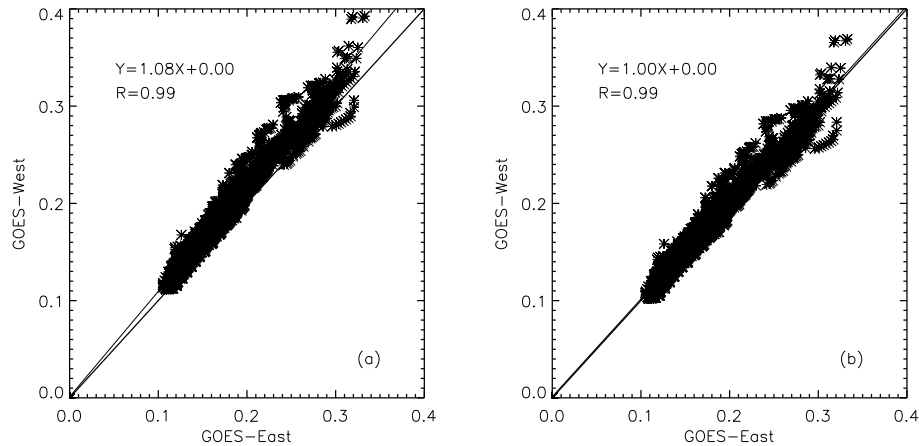


Fig. 11. (a) Scatter plot of GOES-West vs. GOES-East surface reflectance retrievals with mirror symmetry applied at Boulder. (b) Same as the left figure, but the GOES-West TOA reflectance is multiplied by a factor of 0.95.

Title Page

Abstract

Introduction

Conclusions

References

Tables

Figures

◀

▶

◀

▶

Back

Close

Full Screen / Esc

Printer-friendly Version

Interactive Discussion



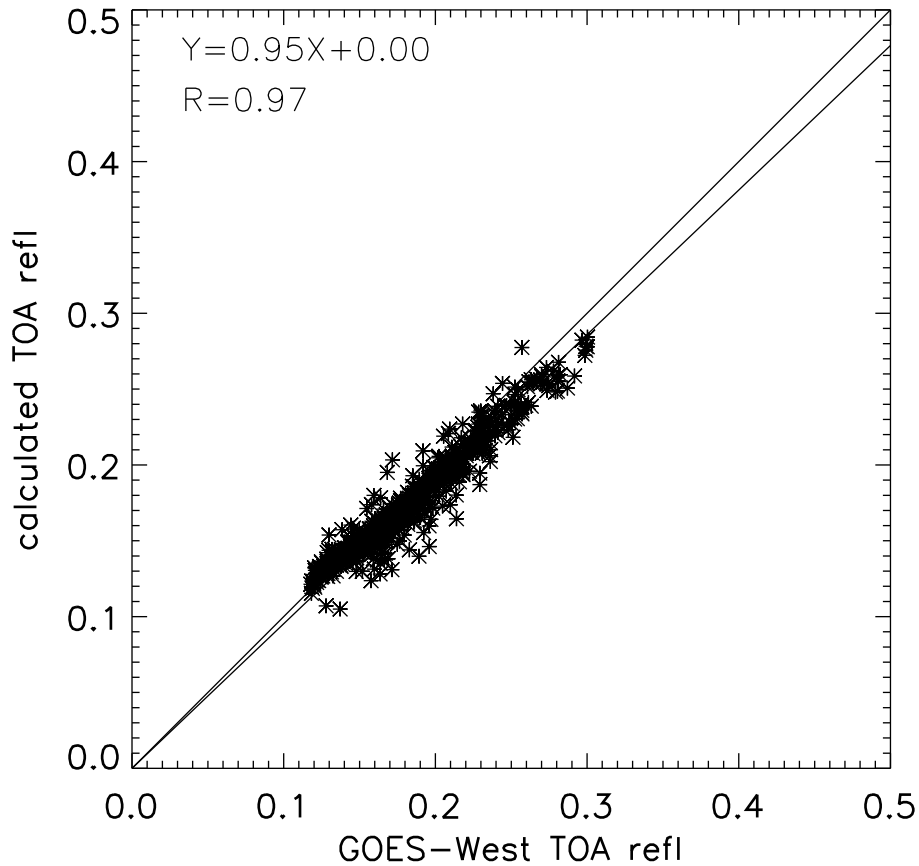


Fig. 12. Scatter plot between calculated TOA reflectance and GOES-West TOA reflectance.

**GOES-East and
GOES-West AOD
retrieval**

H. Zhang et al.

Title Page

Abstract Introduction

Conclusions References

Tables Figures

◀ ▶

◀ ▶

Back Close

Full Screen / Esc

Printer-friendly Version

Interactive Discussion

